

B.E. Biomedical Engineering (BM)

Bio-MEMS 15BM831

Module -3

Engineering Mechanics for Microsystem Design:

Static Bending of Thin plates –

Circular Plates,

Rectangular Plates,

Square Plates with all Edges Fixed,

Mechanical vibrations – General Formulation,

Resonant Vibration,

Design theory of Accelerometers.

Mr. Hemanth Kumar G

Asst. Prof.

Department of BME

ACSCE, Bangalore 74

Module -3

Engineering Mechanics for Microsystems Design

Structural integrity is a primary requirement for any device or engineering system regardless of its size.

The theories and principles of engineering mechanics are used to assess:

- (1) Induced **stresses** in the microstructure by the intended loading, and
- (2) Associated **strains** (or deformations) for the dimensional stability, and the **deformation** affecting the desired performance by this microstructural component.

Accurate assessment of stresses and strains are critical in microsystems design not only for the above two specific purposes, but also is required in the design for signal transduction, as many signals generated by sensors are related to the stresses and strains Induced by the input signals.

Mr. Hemanth Kumar G

Chapter Outline

Static bending of thin plates

Mechanical vibration analysis

Thermomechanical analysis

Fracture mechanics analysis

Thin film mechanics

Overview of finite element analysis

Mechanical Design of Microstructures

Theoretical Bases:

- Linear theory of elasticity for stress analysis
- Newton's law for dynamic and vibration analysis
- Fourier law for heat conduction analysis
- Fick's law for diffusion analysis
- Navier-Stokes equations for fluid dynamics analysis

Mathematical models derived from these physical laws are valid for micro-components $> 1 \mu\text{m}$.

Mechanical Design of Microsystems

Common Geometry of MEMS Components

Beams:

Microrelays, gripping arms in a micro tong, beam spring in micro accelerometers

Plates:

- Diaphragms in pressure sensors, plate-spring in microaccelerometers, etc
- Bending induced deformation generates signals for sensors and relays using beams and plates

Tubes:

Capillary tubes in microfluidic network systems with electro-kinetic pumping (e.g. electro-osmosis and electrophoresis)

Channels:

Channels of square, rectangular, trapezoidal cross-sections in microfluidic network.

- **Component geometry unique to MEMS and microsystems:**
Multi-layers with thin films of dissimilar materials

Recommended Units (SI) and Common Conversion Between SI and Imperial Units in Computation

Units of physical quantities:

Length:	m
Area:	m ²
Volume:	m ³
Force:	N
Weight:	N
Velocity:	m/s
Mass:	g
Mass density:	g/cm ³
Pressure:	Pa

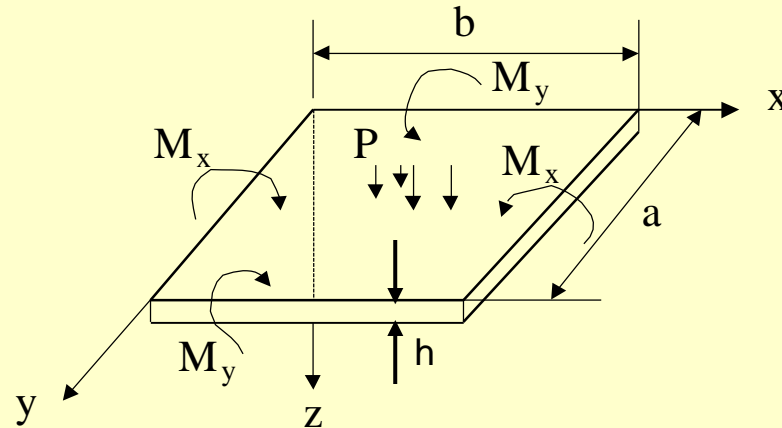
Common conversion formulas:

1 kg = 9.81 m/s²
1 kgf = 9.81 N
1 μm = 10⁻⁶ m
1 Pa = 1 N/m²
1 MPa = 10⁶ Pa = 106 N/m²

1 m = 39.37 in = 3.28 ft
1 N = 0.2252 lb_f (force)
1 kg_f = 2.2 lb_f (weight)
1 MPa = 145.05 psi

Static Bending of Thin Plates

We will deal with a situation with thin plates with fixed edges subjected to laterally applied pressure:



in which, P = applied pressure (MPa)

M_x, M_y = bending moments about respective y and x -axis (N-m/m)

h = thickness of the plate (m)

The governing differential equation for the induced deflection, $w(x,y)$ of the plate is:

$$\frac{\partial^2}{\partial x^2} \left(\frac{\partial^2 w}{\partial x^2} \right) + \frac{\partial^2}{\partial y^2} \left(\frac{\partial^2 w}{\partial y^2} \right) = \frac{p}{D} \quad (4.1)$$

$$\text{with } D = \text{flexural rigidity, } D = \frac{E h^3}{12(1 - \nu^2)} \quad (4.2)$$

in which E = Young's modulus (MPa), and ν = Poisson's ratio

Static Bending of Thin Plates-Cont'd

Once the induced deflection of the plate $w(x,y)$ is obtained from the solution of the governing differential equation (4.1) with appropriate boundary conditions, the bending moments and the maximum associated stresses can be computed by the following expressions:

Bending moments (4.3a,b,c):

$$M_x = -D \frac{\partial^2 w}{\partial x^2} + \nu \frac{\partial^2 w}{\partial y^2}$$

$$M_y = -D \frac{\partial^2 w}{\partial y^2} + \nu \frac{\partial^2 w}{\partial x^2}$$

$$M_{xy} = D(1-\nu) \frac{\partial^2 w}{\partial x \partial y}$$

Bending stresses (4.4a,b,c):

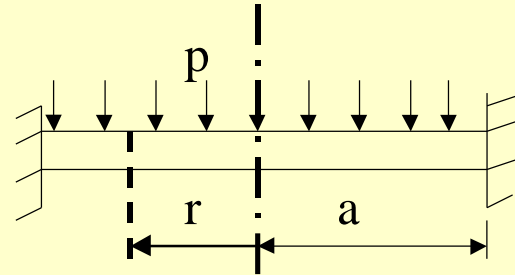
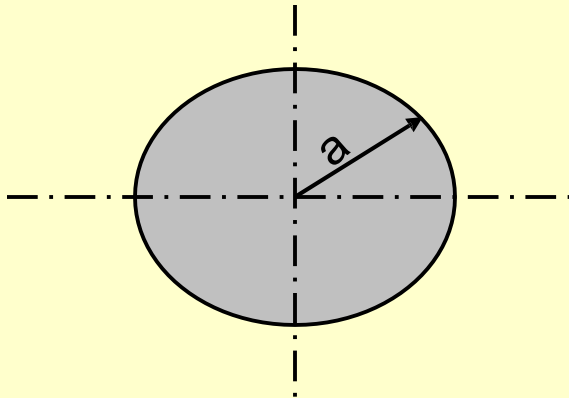
$$(\sigma_{xx})_{\max} = \frac{6(M_x)_{\max}}{h^2}$$

$$(\sigma_{yy})_{\max} = \frac{6(M_y)_{\max}}{h^2}$$

$$(\sigma_{xy})_{\max} = \frac{6(M_{xy})_{\max}}{h^2}$$

Special cases of bending of thin plates

Bending of circular plates



Let W = total force acting on the plate, $W = (\pi a)p$ and $m=1/$

The **maximum stresses** in the r and θ -directions are:

$$(\sigma_{rr})_{\max} = \frac{3W}{4\pi h^2} \quad \text{and} \quad (\sigma_{\theta\theta})_{\max} = \frac{3\nu W}{4\pi h^2} \quad (4.5a,b)$$

Both these **stresses at the center** of the plate is: $\sigma_{rr} = \sigma_{\theta\theta} = \frac{3\nu W}{8\pi h^2} \quad (4.6)$

The **maximum deflection** of the plate occurs at the center of the plate:

$$w_{\max} = -\frac{3W(m^2 - 1)a^2}{16\pi E m^2 h^3} \quad (4.7)$$

Example 4.1 (p.113)

Determine the minimum thickness of the circular diaphragm of a micro pressure sensor made of Silicon as shown in the figure with conditions:

Diameter $d = 600 \mu\text{m}$; Applied pressure $p = 20 \text{ MPa}$

Yield strength of silicon $\sigma_y = 7000 \text{ MPa}$

$E = 190,000 \text{ MPa}$ and $\nu = 0.25$.

Solution:

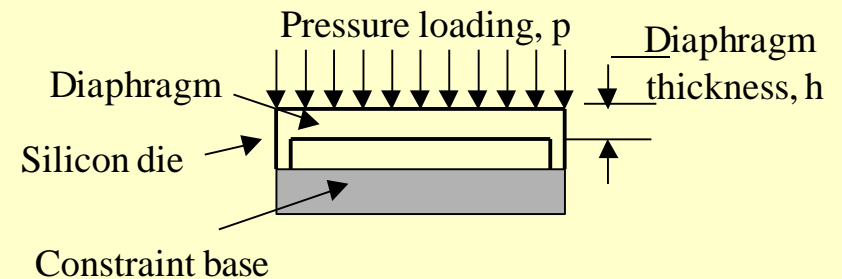
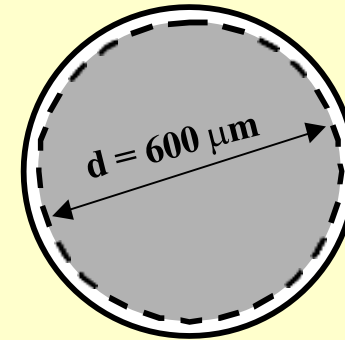
$$(\sigma_{rr})_{\max} = \frac{3W}{4\pi h^2} \longrightarrow h = \sqrt{\frac{3W}{4\pi(\sigma_{rr})_{\max}}}$$

$$(\sigma_{\theta\theta})_{\max} = \frac{3\nu W}{4\pi h^2} \longrightarrow h = \sqrt{\frac{3\nu W}{4\pi(\sigma_{\theta\theta})_{\max}}}$$

Use the condition that $\sigma_{rr} < \sigma_y = 7000 \text{ MPa}$ and $\sigma_{\theta\theta} < \sigma_y = 7000 \text{ MPa}$, and

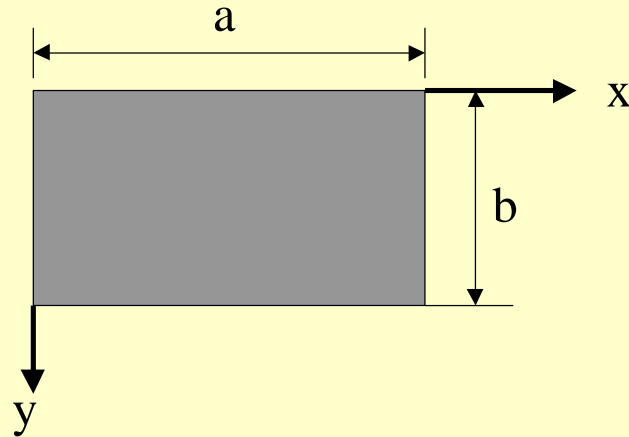
$W = (\pi a^2)p = 3.14 \times (300 \times 10^{-6})^2 \times (20 \times 10^6) = 5.652 \text{ N}$, we get the minimum thickness of the “plate” to be:

$$h = \sqrt{\frac{3 \times 5.652}{4 \times 3.14 \times (7000 \times 10^6)}} = 13.887 \times 10^{-6} \text{ m} \quad \text{or } 13.887 \mu\text{m}$$



Special cases of bending of thin plates-Cont'd

Bending of rectangular plates



The maximum stress and deflection in the plate are:

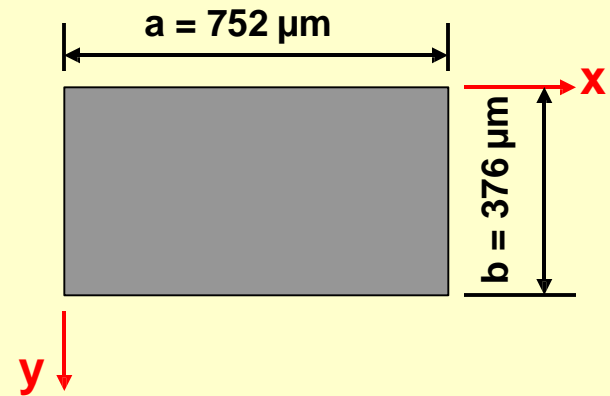
$$(\sigma_{yy})_{\max} = \beta \frac{pb^2}{h^2} \quad \text{and} \quad w_{\max} = \alpha \frac{pb^4}{Eh^3} \quad (4.8 \text{ and } 4.9)$$

in which coefficients α and β can be obtained from Table 4.1:

a/b	1	1.2	1.4	1.6	1.8	2.0	∞
α	0.0138	0.0188	0.0226	0.0251	0.0267	0.0277	0.0284
β	0.3078	0.3834	0.4356	0.4680	0.4872	0.4974	0.5000

Example 4.2 (p.115)

A rectangular diaphragm, $13.887 \mu\text{m}$ thick has the plane dimensions as shown in the figure. The diaphragm is made of silicon. Determine the maximum stress and deflection when it is subjected to a normal pressure, $P = 20 \text{ MPa}$. All 4 edges of the diaphragm are fixed.



Solution:

We will first determine $\alpha = 0.0277$ and $\beta = 0.4974$ with $a/b = 752/376 = 2.0$ from the Given Table. Thus, from available formulas, we get the **maximum stress**:

$$(\sigma_{yy})_{\max} = \beta \frac{p b^2}{h^2} = 0.4974 \frac{(20 \times 10^6)(376 \times 10^{-6})^2}{(13.887 \times 10^{-6})^2} = 7292.8 \times 10^6 \text{ Pa}$$

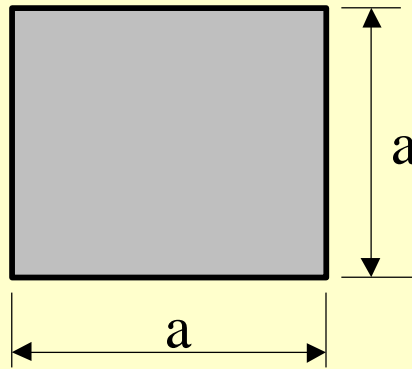
and the **maximum deflection**:

$$w_{\max} = -\alpha \frac{p b^4}{E h^3} = -\alpha \frac{p b^3}{E h} = -\frac{0.0277 \times (20 \times 10^6) \times 376 \times 10^{-6}}{190000 \times 10^6} \frac{376 \times 10^{-6}^3}{13.887 \times 10^{-6}} = -21.76 \times 10^{-6} \text{ m}$$

at the center (centroid) of the plate

Special cases of bending of thin plates-Cont'd

Bending of square plates:



The maximum stress occurs at the middle of each edge: $\sigma_{\max} = \frac{0.308 p a^2}{h^2}$ (4.10)

The maximum deflection occurs at the center of the plate: $w_{\max} = -\frac{0.0138 p a^4}{E h^3}$ (4.11)

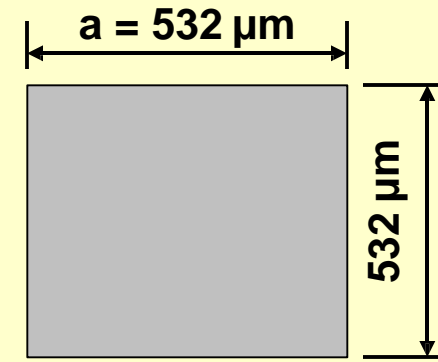
The stress and strain at the center of the plate are:

$$\sigma = \frac{6p(m+1)a^2}{47mh^2} \quad \text{and} \quad \varepsilon = \frac{1-\nu}{E} \sigma \quad (4.12 \text{ and } 4.13)$$

Square diaphragm (idealized as a square plate) is the sensing element in many micro pressure sensors

Example 4.3 (p.116)

Determine the maximum stress and deflection in a square plate made of silicon when is subjected to a pressure loading, $p = 20 \text{ MPa}$. The plate has edge length, $a = 532 \text{ }\mu\text{m}$ and a thickness, $h = 13.887 \text{ }\mu\text{m}$.



Solution:

From the given formulas, we have the maximum stress to be:

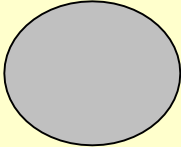


$$\sigma_{\max} = \frac{0.308 p a^2}{h^2} = \frac{0.308 \times (20 \times 10^6) (532 \times 10^{-6})^2}{(13.887 \times 10^{-6})^2} = 9040 \times 10^6 \text{ Pa}$$

and the maximum deflection:

$$w_{\max} = -\frac{0.0138 p a^4}{E h^3} = -\frac{0.0138 p a^3}{E h} =$$
$$-\frac{0.0138 (20 \times 10^6) \times 532 \times 10^{-6}}{190000 \times 10^6} \times \frac{532 \times 10^{-6}}{13.887 \times 10^{-6}} = -43 \times 10^{-6} \text{ m} \quad \text{or } w_{\max} = 43 \text{ }\mu\text{m}$$

Geometric effect on plate bending

Comparison of results obtained from Example 4.1, 4.2 and 4.3 for plates made of silicon having **same surface area and thickness**, subjected to the **same applied pressure** indicate significant difference in the induced maximum stresses and deflections:

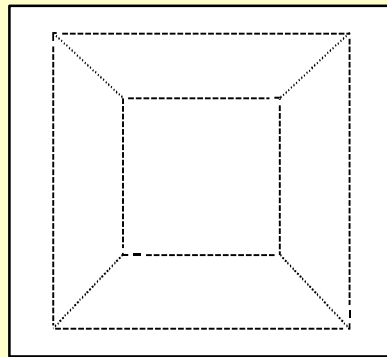
Geometry	Maximum Stress (MPa)	Maximum Deflection (μm)
	7000	55.97
	7293	21.76
	9040 highest stress output	43.00

The circular diaphragm is most favored from design engineering point of view. The square diaphragm has the highest induced stress of all three cases. It is favored geometry for pressure sensors because the high stresses generated by applied pressure loading – result in high sensitivity..

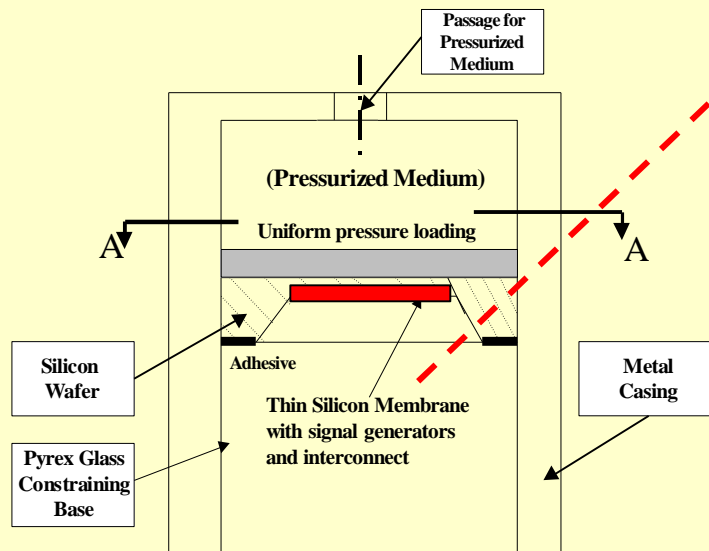
Example 4.4

(p. 118)

Determine the maximum stress and deflection in a square diaphragm used in a micro pressure sensor as shown in the figure. The maximum applied pressure is $p = 70 \text{ MPa}$.



View on Section "A-A"

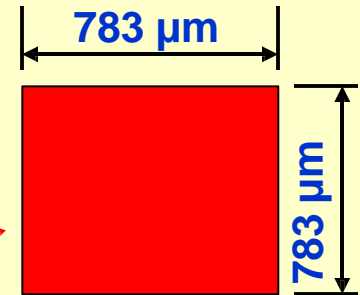
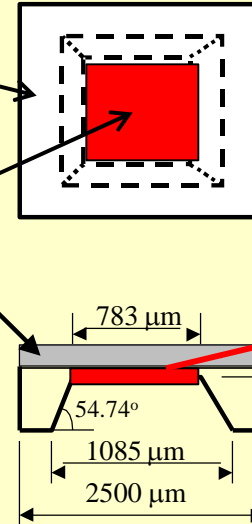


Detail of the Silicon die and diaphragm:

Silicon die

Diaphragm

Uniform pressure loading: 70 MPa



Thickness $h = 266 \mu\text{m}$

By using the formulas for square plates, we get:

$$\sigma_{\max} = \frac{0.308 \times 70 \times 10^6 \times (783 \times 10^{-6})^2}{(266 \times 10^{-6})^2} = 186.81 \text{ MPa}$$

and the maximum deflection:

$$w_{\max} = - \frac{0.0138 \times 70 \times (783 \times 10^{-6})^4}{190000 \times (266 \times 10^{-6})^3} = -10153 \times 10^{-11} \text{ m}$$

or $0.1015 \mu\text{m}$ (downward)

Mechanical Vibration Analysis

Mechanical vibration principle is used in the design of micro-accelerometer, which is a common MEMS device for measuring forces induced by moving devices.

Microaccelerometers are used as the sensors in automobile air bag deployment systems.

We will outline some key equations involved in mechanical vibration analysis and show how they can be used in microaccelerometer design.

Overview of Simple Mechanical Vibration Systems

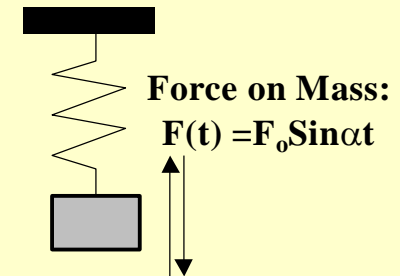
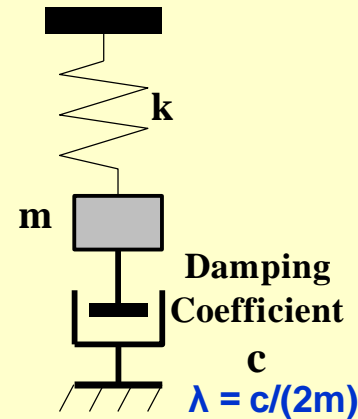
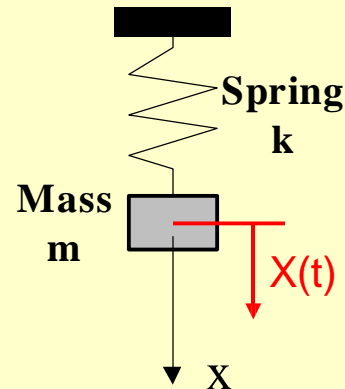
(a) Free vibration: (b) Damped vibration: (c) Forced vibration:

Circular frequency:

$$\omega = \sqrt{\frac{k}{m}}$$

Natural frequency:

$$f = \frac{\omega}{2\pi}$$



$X(t)$ = instantaneous position of the mass, or the displacement of the mass at time t .
 $X(t)$ is the solution of the following differential equation with C_1 and C_2 being constants:

$$m \frac{d^2 X(t)}{dt^2} + kX(t) = 0 \quad \text{Eq. (4.14) for Case (a)} \longrightarrow X(t) = C_1 \cos(\omega t) + C_2 \sin(\omega t)$$

$$m \frac{d^2 X(t)}{dt^2} + c \frac{dX(t)}{dt} + kX(t) = 0 \quad \text{Eq. (4.19) for Case (b)} \longrightarrow$$

$$X(t) = e^{-\lambda t} (C_1 e^{t\sqrt{\lambda^2 - \omega^2}} + C_2 e^{-t\sqrt{\lambda^2 - \omega^2}}) \quad \text{for } \lambda^2 - \omega^2 > 0$$

$$X(t) = e^{-\lambda t} (C_1 + C_2 t) \quad \text{for } \lambda^2 - \omega^2 = 0$$

$$X(t) = e^{-\lambda t} (C_1 \cos \sqrt{\omega^2 - \lambda^2} t + C_2 \sin \sqrt{\omega^2 - \lambda^2} t) \quad \text{for } \lambda^2 - \omega^2 < 0$$

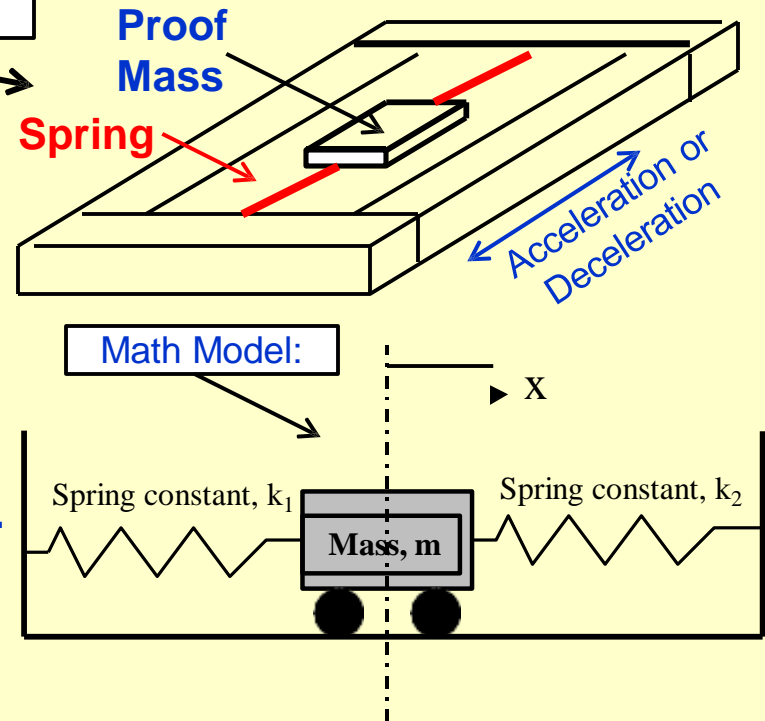
$$m \frac{d^2 X(t)}{dt^2} + kX(t) = F_0 \sin(\alpha t) \quad \text{Eq (4.21) for Case (c)} \longrightarrow X(t) = \frac{F_0}{\omega(\omega^2 - \alpha^2)} (-\alpha \sin \omega t + \omega \sin \alpha t)$$

In a special case of which $\alpha = \omega \longrightarrow$ **Resonant vibration:** $X(t) = \frac{F_0}{2\omega^2} \sin \omega t - \frac{F_0}{2\omega} t \cos \omega t$

Example 4.6 (p.121)

A typical μ -accelerometer:

Determine the amplitude and frequency of vibration of a 10-mg mass attached to two springs as shown in the figure. The mass can vibrate freely without friction between the rollers and the supporting floor. Assume that the springs have same spring constant $k_1 = k_2 = k = 6 \times 10^{-5} \text{ N/m}$ in both tension and compression. The vibration begins with the mass being pulled to the right with an amount of $\delta_{st} = 5 \mu\text{m}$. (as induced by acceleration or deceleration)



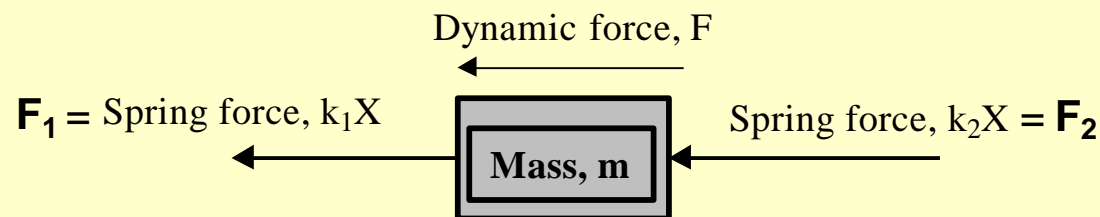
Solution:

We envisage that the mass in motion is subjected to two spring forces:

One force by stretching the spring ($F_1 = k_1 x$) + the other by compressing ($F_2 = k_2 x$).

Also If the spring constants of the two springs are equal, ($k_1 = k_2$).

And also each spring has equal magnitudes of its spring constants in tension and Compression. We will have a situation:



In which $F_1 = F_2$, This is the situation that is called “Vibration with balanced force”

Example 4.6-Cont'd

Since the term $kX(t)$ in the differential equation in Eq. (4.14) represent the “spring force” acting on the vibrating mass, and the spring force in this case is twice the value.

We may replace the term $kX(t)$ in that equation with $(k+k)X(t)$ or $2kX(t)$ as:

$$m \frac{d^2 X(t)}{dt^2} + 2k X(t) = 0$$

with the conditions: $X(0) = \delta_{st} = 5 \mu\text{m}$, and $\left. \frac{dX(t)}{dt} \right|_{t=0} = 0$ (zero initial velocity)

The general solution of the differential equation is: $X(t) = C_1 \cos(\omega t) + C_2 \sin(\omega t)$, in which $C_1 = \delta_{st} = 5 \times 10^{-6} \text{ m}$ and $C_2 = 0$ as determined by the two conditions.

Thus, the instantaneous position of the mass is: $X(t) = 5 \times 10^{-6} \cos(\omega t)$ meter

The corresponding maximum displacement is $X_{\max} = 5 \times 10^{-6} \text{ m}$

The circular frequency, ω in this case is:

$$\omega = \sqrt{\frac{2k}{m}} = \sqrt{\frac{(6+6) \times 10^{-5}}{10^{-5}}} = 3.464 \text{ rad/s}$$

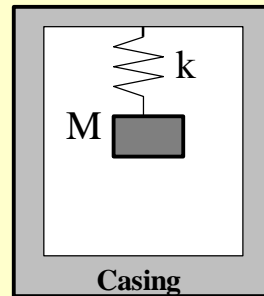
Microaccelerometers

Micro accelerometers are used to measure the **acceleration (or deceleration)** of a moving solid (e.g. a device or a vehicle), and thereby relate the acceleration to the associated dynamic force using **Newton's 2nd law: $F(t) = M a(t)$** , in which M = mass of the moving solid and **$a(t)$ = the acceleration** at time t .

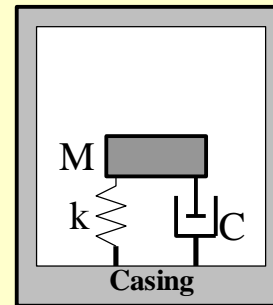
An accelerator requires: **a proof mass (m)**, **a spring (k)**, and **damping medium (c)**, in which k = spring constant and c = damping coefficient.

Early design of microaccelerators have the following configurations:

Conventional
accelerometers →

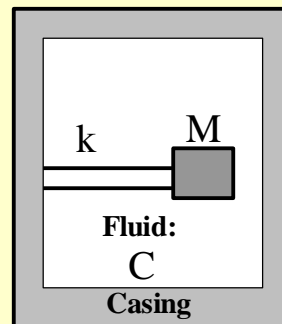


(a) Spring-mass

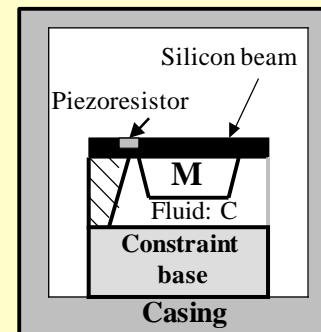


(b) Spring-mass-dashpot

Microaccelerometers →



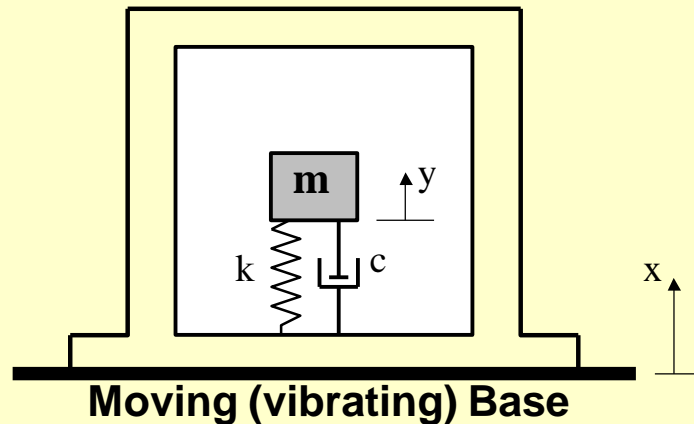
(c) Beam-Mass



(d) Beam-attached mass

Design Theory of Accelerometers

In a real-world application, the accelerometer is attached to a moving solid. We realize that the **amplitude of the vibrating proof mass in the accelerometer** may not necessarily be in phase with the **amplitude of vibration of the moving solid (the base)**.



$x(t)$ = the amplitude of vibration of the base

Assume $x(t) = X \sin(\omega t)$ – a harmonic motion

$y(t)$ = the amplitude of vibration of proof mass in the accelerometer from its initial static equilibrium position.

$z(t)$ = the relative (or net) motion of the proof mass, m

Hence $z(t) = y(t) - x(t)$ (4.26)

The governing differential equation for $z(t)$ is:

$$m\ddot{z}(t) + c\dot{z}(t) + kz(t) = mX\omega^2 \sin\omega t \quad (4.29)$$

Once $z(t)$ is obtained from solving the above equation with appropriate initial conditions, we may obtain the acceleration of the proof mass in a relative movement as:

$$\ddot{z}(t) = \frac{d^2 z(t)}{dt^2}$$

Design Theory of Accelerometers-Cont'd

The solution of $z(t)$ with initial conditions: $z(0) = 0$ and $\left. \frac{dz(t)}{dt} \right|_{t=0} = 0$ is:

$$z(t) = Z \sin(\omega t - \Phi) \quad (4.30)$$

in which the **maximum magnitude**, Z of $z(t)$ is:

$$Z = \frac{\omega^2 X}{\sqrt{\frac{k}{m} - \omega^2 - \frac{\omega^2 c^2}{m}}} \quad (4.31a)$$

where X = maximum amplitude of vibration of the base. The phase angle difference, Φ between the input motion of $x(t)$ and the relative motion, $z(t)$ is:

$$\phi = \tan^{-1} \frac{\frac{\omega c}{m}}{\frac{k}{m} - \omega^2} \quad (4.31b)$$

Design Theory of Accelerometers-Cont'd

An alternative form for the maximum amplitude of the relative vibration of the proof mass in the accelerometer, Z is:

$$Z = \frac{\omega^2 X}{\omega_n^2 \sqrt{1 - \left(\frac{\omega}{\omega_n}\right)^2 + 2h \frac{\omega}{\omega_n}}} \quad (4.32a)$$

where ω = frequency of the vibrating base; ω_n is the circular natural frequency of the accelerometer with:

$$\omega_n = \sqrt{\frac{k}{m}}$$

The parameter, $h = c/c_c$ = the ratio of the damping coefficients of the damping medium in the micro accelerometer to its critical damping with $c_c = 2m\omega_n$

For the case of which the frequency of the vibrating base, ω is much smaller than the natural frequency of the accelerometer, ω_n , i.e. $\omega \ll \omega_n$:

$$Z \approx \frac{a_{base, \max}}{\omega_n^2} \quad (4.33)$$

Design of Accelerometers

The engineer may follow the following procedure in the design of appropriate microaccelerometer for a specific application:

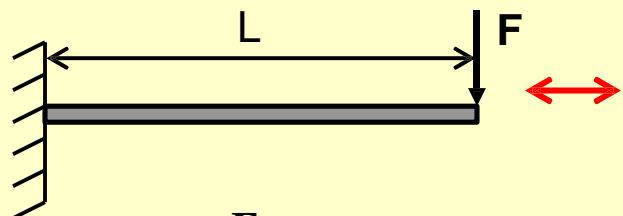
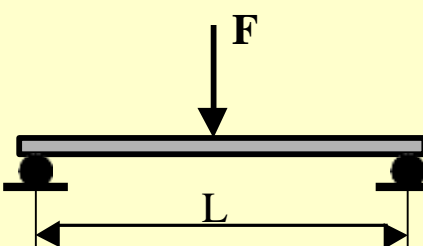
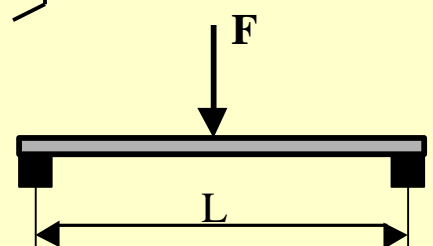
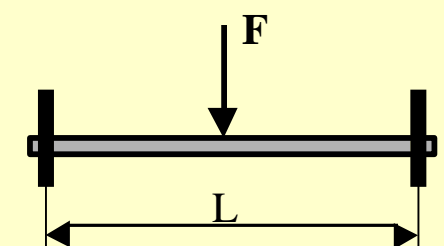
- (1) Set the **target maximum amplitude of vibration, X of the base** (e.g., a vehicle or a machine) and the **anticipated frequency of vibration, i.e. ω** .
- (2) Select the parameters: **m , k , c** and calculate ω_n and h .
- (3) Compute the maximum relative amplitude of vibration of the proof mass, **Z** using the available formulas.
- (4) Check if the computed Z is within the range of measurement of the **intended transducer**, e.g. piezoresistors, piezoelectric, etc.
- (5) Adjust the parameters in Step (2) if the computed Z is too small to be measured by the intended transducer.

Design of Accelerometers-Cont'd

Spring constant of simple beams

Simple beams are commonly used to substitute the coil springs in microaccelerometers. It is thus necessary to calculate the “equivalent spring constant” of these beam springs.

Since the spring constant of an elastic solid, whether it is a coil spring or other geometry, is defined as **$k = \text{Force/Deflection}$** (at which the force is applied), we may derive the spring constant for the three simple beam configurations to be:


$$k = \frac{\text{Applied force, } F}{\text{Induced deflection, } \delta} = \frac{3EI}{L^3}$$

$$k = \frac{48EI}{L^3}$$

$$k = \frac{192EI}{L^3}$$

in which **E** = Young's modulus; **I** = section moment of inertia of beam cross-section.

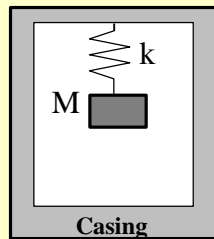
Design of Accelerometers-Cont'd

Damping coefficients

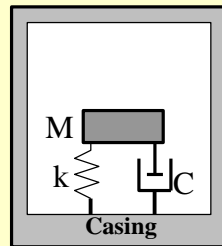
In microaccelerometers, the friction between the immersed fluid and the contacting surfaces of the moving proof mass provides damping effect.

There are two types of “damping” induced by this affect:

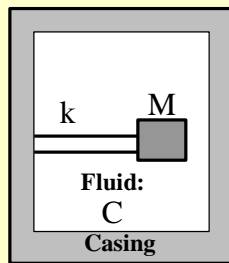
(a) Squeeze film damping:



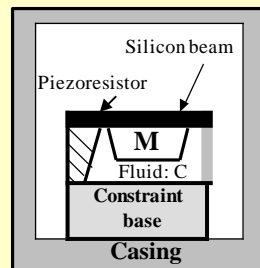
(a) Spring-mass



(b) Spring-mass-dashpot

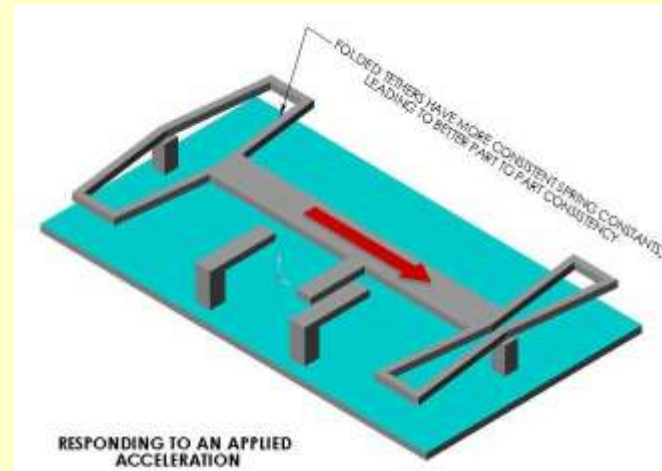


(c) Beam-Mass



(d) Beam-attached mass

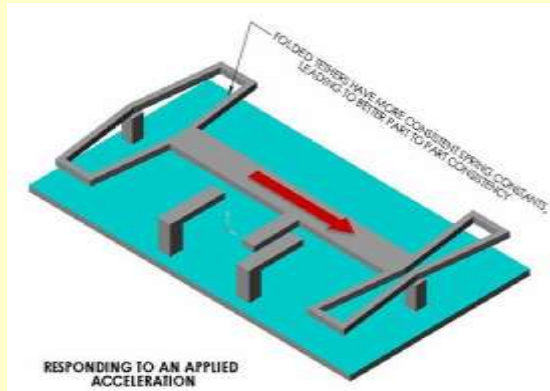
(b) Micro damping in shear:



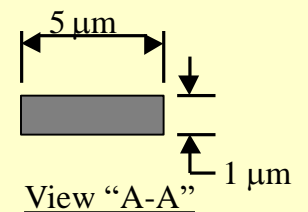
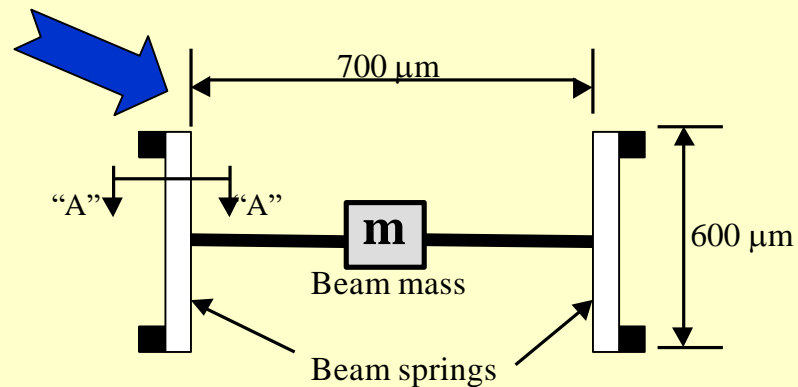
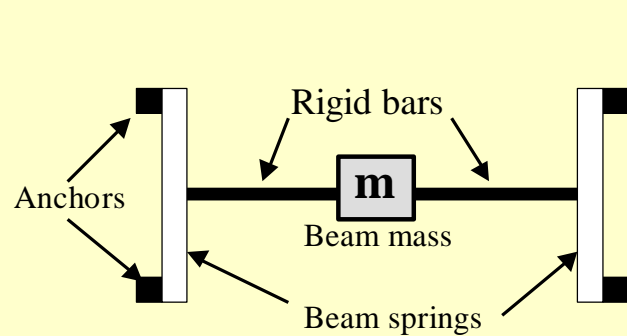
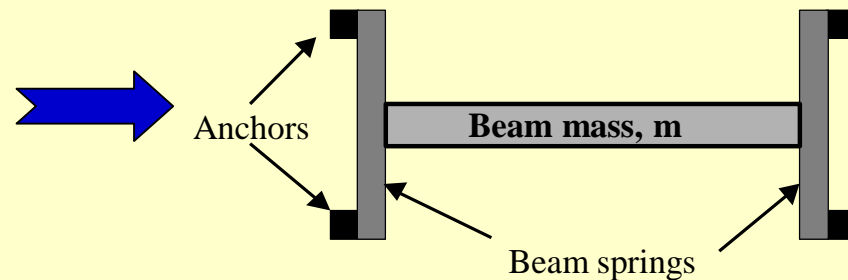
Numerical values of damping coefficients depend on the geometry of the vibrating solid components and the fluid that surround them.

Example 4.10 (p.133)

Determine the displacement of the proof mass from its neutral equilibrium position of a balanced-force microaccelerometer illustrated below:



The structure of this accelerometer can be graphically represented below:



With: $b = 10^{-6} \text{ m}$, $B = 100 \times 10^{-6} \text{ m}$, $L = 600 \times 10^{-6} \text{ m}$ and $L_b = 700 \times 10^{-6} \text{ m}$, we have from Example 4.9 the moment of inertia of beam spring cross-section to be:

$$I = 10.42 \times 10^{-24} \text{ m}^4$$

For simply-support beam spring: $k = 0.44 \text{ N/m}$, $\omega_n = 23,380 \text{ rad/s}$

For rigidly fixed beam spring: $k = 1.76 \text{ N/m}$ and $\omega_n = 147,860 \text{ rad/s}$

Assume the “rigidly held beam spring case is adopted, the equation of motion of the proof mass is:

$$\frac{d^2 X(t)}{dt^2} + \omega^2 X(t) = 0$$

with initial conditions: $X(t)|_{t=0} = 0$ initial position

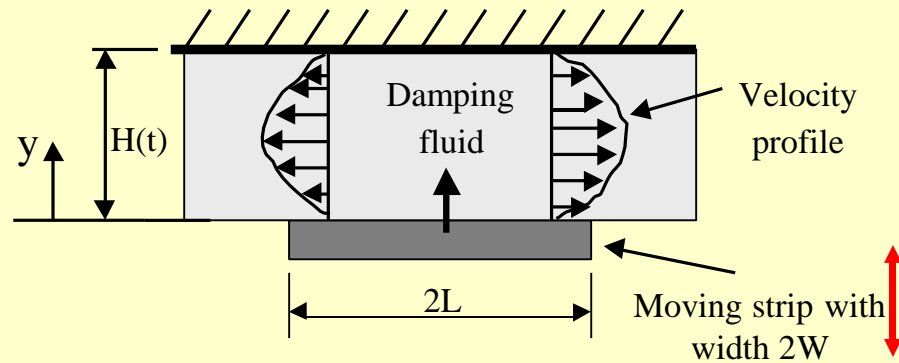
, and $\left. \frac{dX(t)}{dt} \right|_{t=0} = 50 \text{ km/h} = 13.8888 \text{ m/s}$ initial velocity

The solution of the equation of motion with the given initial conditions is:

$$X(t) = 9.3932 \times 10^{-5} \sin(147.86t)$$

leading to $X(1 \text{ ms}) = -2.597 \times 10^{-5} \text{ m}$ or $26 \text{ }\mu\text{m}$ opposite to the direction of deceleration.

(a) Damping coefficient in a squeeze film:



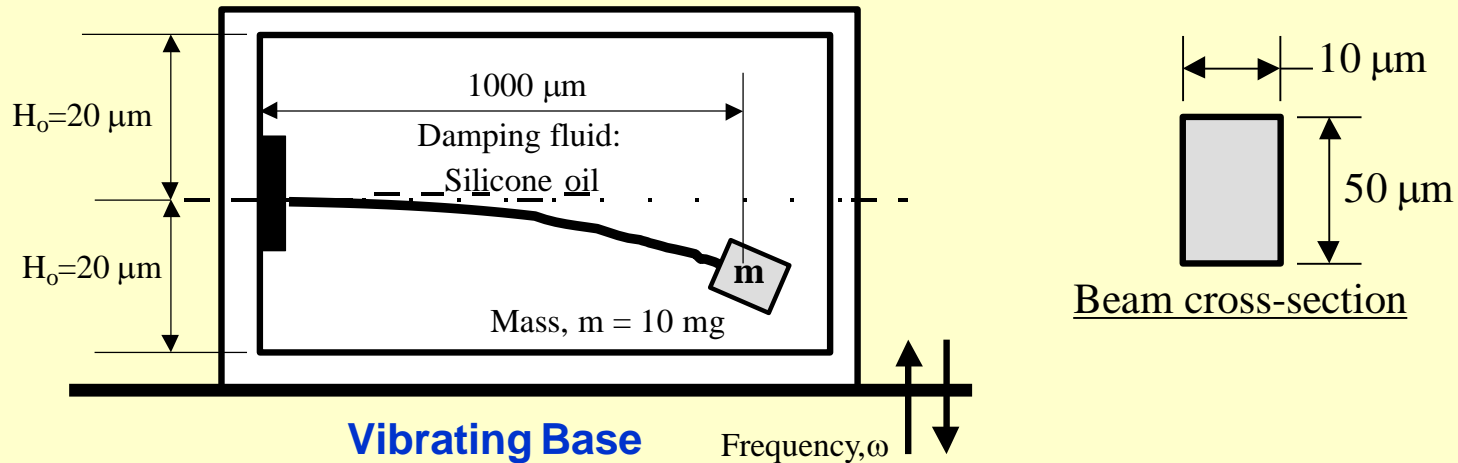
The **damping coefficient** can be found to be: $c = 16 f \left(\frac{W}{L} \right)^3 W^3 L H_o^3$
 where H_o = nominal thickness of the thin film.

The function, $f \left(\frac{W}{L} \right)$ can be obtained by the following Table 4.2:

$\frac{W}{L}$	$f \left(\frac{W}{L} \right)$	$\frac{W}{L}$	$f \left(\frac{W}{L} \right)$
0	1.00	0.6	0.60
0.1	0.92	0.7	0.55
0.2	0.85	0.8	0.50
0.3	0.78	0.9	0.45
0.4	0.72	1.0	0.41
0.5	0.60		

Example 4.11 (p.136)

Estimate the damping coefficient of a micro accelerometer using a cantilever beam spring as illustrated.

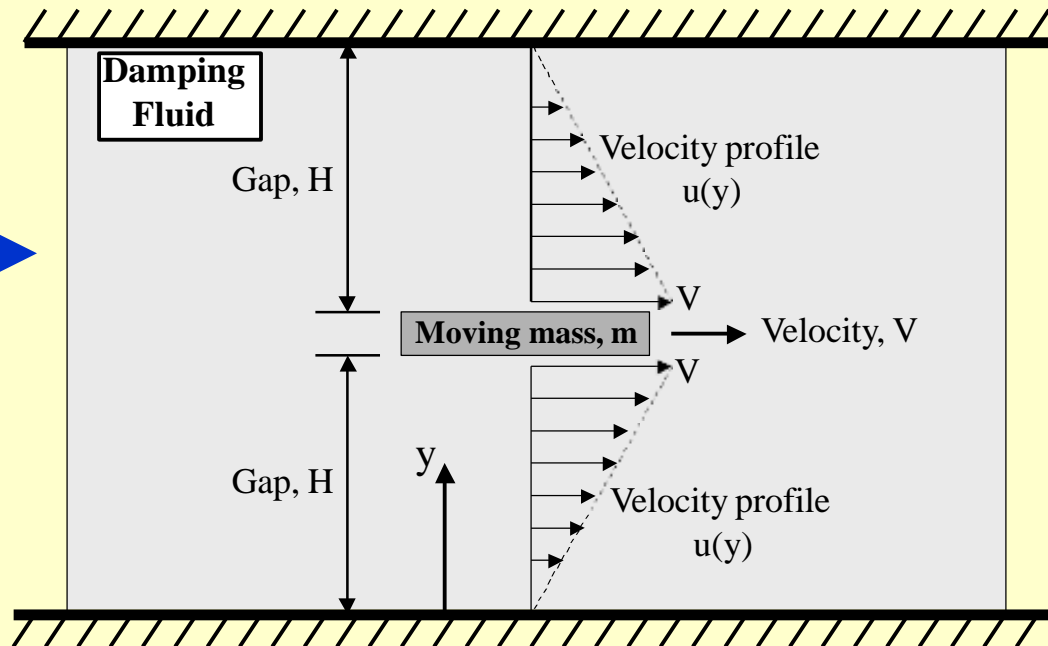
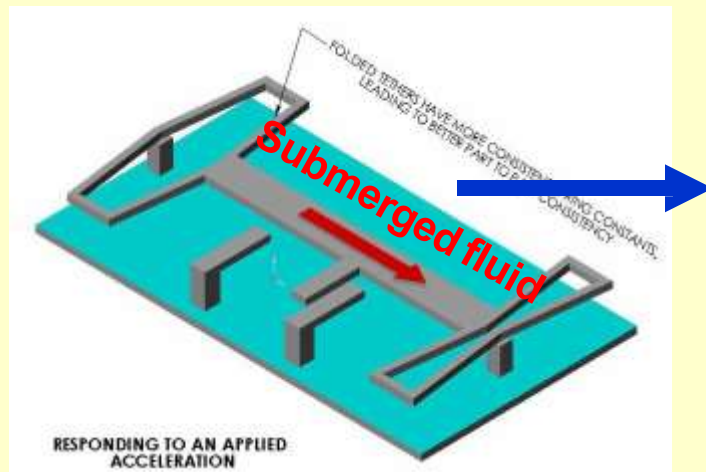


We have the beam dimensions as: $2L = 1000 \times 10^{-6}\ \text{m}$ and $2W = 10 \times 10^{-6}\ \text{m}$ →

$W/L = 0.01$ → $F(W/L) = 0.992$ from Table 4.2.

The nominal film thickness, $H_o = 20 \times 10^{-6}\ \text{m}$. From Eq. (4.38) we get: $c = 8 \times 10^{-33}\ \text{N-s/m}$.

(b) Micro damping in shear:



The damping coefficient, c may be computed from the following expression:

$$c = \frac{F_D}{V} = \frac{2\mu Lb}{H} \quad \text{N-s/m} \quad (4.43)$$

where L = length of the beam (m); b = the width of the beam (m); H = gaps (m)
 μ = dynamic viscosity of the damping fluid (N-s/m²), see Table below.

Dynamic Viscosity for Selected Fluids (in 10^{-6} N-s/m²)

A. Compressible fluids:

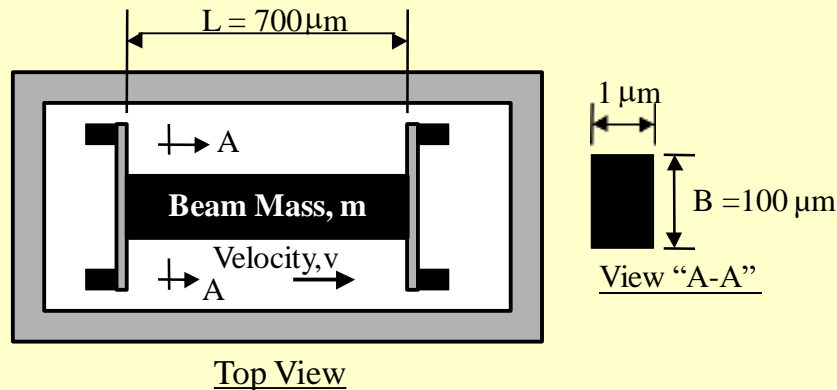
	0°C	20°C	60°C	100°C	200°C
Air	17.08	18.75	20.00	22.00	25.45
Helium	18.60	19.41	21.18	22.81	26.72
Nitrogen	16.60	17.48	19.22	20.85	24.64

B. Non-compressible fluids:

	0°C	20°C	40°C	60°C	80°C
Alcohol	1772.52	1199.87	834.07	591.80	432.26
Kerosene	2959.00	1824.23	1283.18	971.96	780.44
Fresh water	1752.89	1001.65	651.65	463.10	351.00
Silicone oil*		740			

Example 4.12 (p.139)

Estimate the damping coefficient in a balanced-force microaccelerometer as illustrated, with (a) air, and (b) silicone oil as damping media. The sensor operates at 20°C.



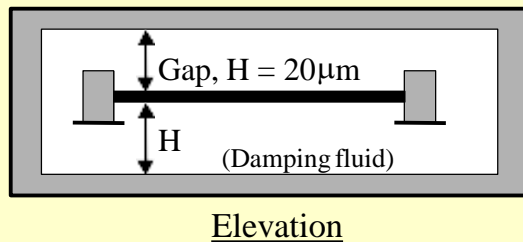
Eq. (4.43) is used for the solutions.

We have $L = 700 \times 10^{-6} \text{ m}$ and $b = 5 \times 10^{-6} \text{ m}$ and the gap, $H = 10 \times 10^{-6} \text{ m}$.

The dynamic viscosities for air and silicone oil at 20°C may be found from Table 4.3 to be:

$$\mu_{\text{air}} = 18.75 \times 10^{-6} \text{ N-s/m}^2, \text{ and}$$

$$\mu_{\text{si}} = 740 \times 10^{-6} \text{ N-s/m}^2$$



Thus, the damping coefficient with air is:

$$c = \frac{2 \mu_{\text{air}} L b}{H} = \frac{2(18.75 \times 10^{-6})(700 \times 10^{-6})(100 \times 10^{-6})}{20 \times 10^{-6}} = 2.625 \times 10^{-12} \text{ N-s/m}$$

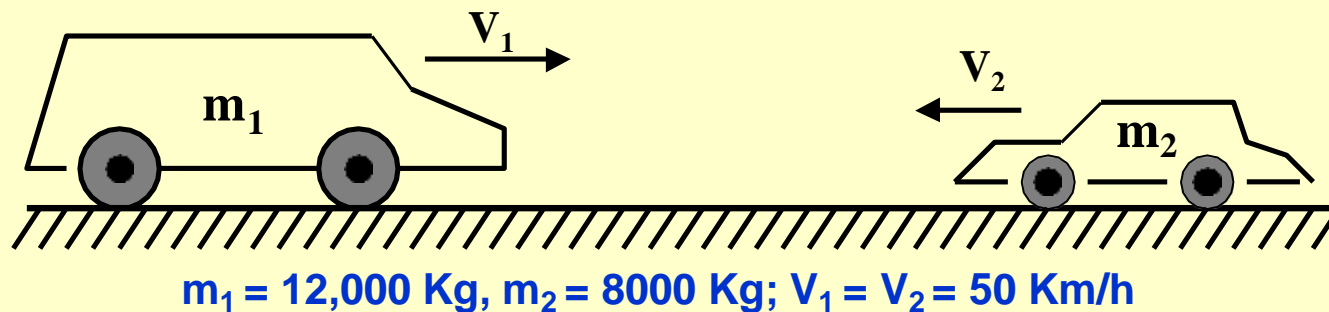
and the damping coefficient with silicone oil is:

$$c = \frac{2 \mu_{\text{si}} L b}{H} = \frac{2(740 \times 10^{-6})(700 \times 10^{-6})(100 \times 10^{-6})}{20 \times 10^{-6}} = 1.036 \times 10^{-10} \text{ N-s/m}$$

Example 4.14 Design of an inertia sensor for airbag deployment system in automobiles (p.142)

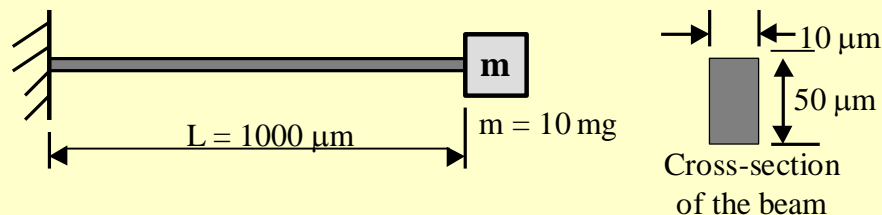
Two vehicles with respective masses, m_1 and m_2 traveling in opposite directions at velocities V_1 and V_2 as illustrated. Each vehicle is equipped with an inertia sensor (or micro accelerometer) built with cantilever beam as configured in Example 4.8.

Estimate the *deflection* of the proof mass in the sensor in vehicle 1 with mass m_1 , and also the *strain* in the two piezoresistors embedded underneath the top and bottom surfaces of the beam near the support after the two vehicles collide.



Solution:

Let us first look into the property of the “beam spring” used in Example 4.8, and have:

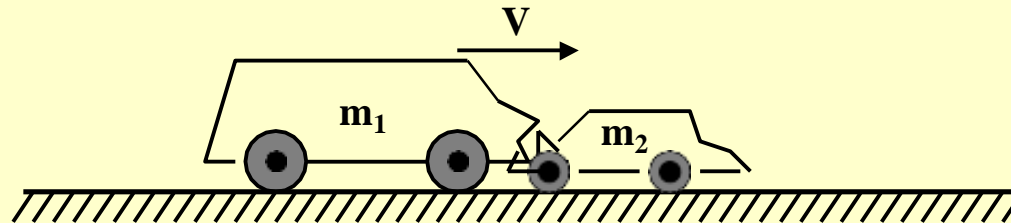


$$I = \frac{(10 \times 10^{-6})(50 \times 10^{-6})^3}{12} = 0.1042 \times 10^{-18} \text{ m}^4$$

$$k = \frac{3(190000 \times 10^6)(0.1042 \times 10^{-18})}{(1000 \times 10^{-6})^3} = 59.39 \text{ N/m}$$

$$\omega_n = \sqrt{\frac{k}{m}} = \sqrt{\frac{59.39}{10^{-5}}} = 2437 \text{ Rad/s}$$

Postulation: The two vehicles will tangle together after the collision, and the entangled vehicles move at a velocity V as illustrated:



Thus, by **law of conservation of momentum**, we should have the velocity of the entangled vehicles to be:

$$V = \frac{m_1 V_1 - m_2 V_2}{m_1 + m_2} = \frac{12000 \times 50 - 8000 \times 50}{12000 + 8000} = 10 \quad \text{Km/h}$$

The decelerations of the two vehicles are:

$$a = \frac{V - V_1}{\Delta t} \quad \text{for vehicle with } m_1, \text{ and } a = \frac{V - V_2}{\Delta t} \quad \text{for vehicle with } m_2$$

in which Δt = time required for deceleration.

Let us **assume** that it takes 0.5 second for vehicle 1 to decelerate from 50 Km/hr to 10 Km/hr after the collision. Thus the time for deceleration of the vehicle m_1 is $\Delta t = 0.5$ second, in the above expressions.

We may thus compute the deceleration of vehicle m1 to be:

$$\ddot{x} = a_{base} = \frac{(10 - 50) \times 10^3 / 3600}{0.5} = -22.22 \text{ m/s}^2$$

Let ω = frequency of vibration of the vehicles.

Assume that $\omega \ll \omega_n$, (ω_n = the natural frequency of the accelerometer = 2437 rad/s²).

Consequently, we may approximate the amplitude of vibration of the proof mass in the accelerometer using Eq. (4.33) as:

$$Z = \frac{a_{base}}{\omega_n^2} = -\frac{22.22}{(2437)^2} = 3.74 \times 10^{-6} \text{ m, or } 3.74 \text{ } \mu\text{m}$$

We thus have the maximum deflection of the cantilever beam of 3.74 μm at the free end in the accelerometer. The equivalent force acting at the free-end is:

$$F = \frac{3EI Z}{L^3} = \frac{3(1.9 \times 10^{11})(0.1042 \times 10^{-18})(3.74 \times 10^{-6})}{(1000 \times 10^{-6})^3} = 2.2213 \times 10^{-4} \text{ N}$$

From which, we may compute the **maximum bending moment** at the support to be:

$M_{\max} = FL$ in which L is the length of the beam. The numerical value of M_{\max} is:

$$M_{\max} = 2.2213 \times 10^{-4} \times 10^{-3} = 2.2213 \times 10^{-7} \quad \text{N-m}$$

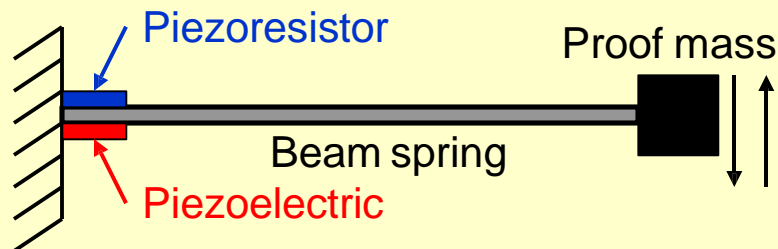
The corresponding maximum stress, σ_{\max} is:

$$\sigma_{\max} = \frac{M_{\max} C}{I} = \frac{(2.2213 \times 10^{-7})(25 \times 10^{-6})}{0.1042 \times 10^{-18}} = 532.95 \times 10^5 \text{ N/m}^2 \text{ or Pa}$$

and the corresponding max. strain is obtained by using the Hooke's law to be:

$$\varepsilon_{\max} = \frac{\sigma_{\max}}{E} = \frac{53.30 \times 10^5}{190 \times 10^9} = 0.281 \times 10^{-4} = 0.0281\%$$

Depending on the transducer used in the microaccelerometer, the maximum stress, σ_{\max} can produce a **resistance change** in the case of “**piezoresistors**”. Alternatively, the maximum strain, ε_{\max} will produce a **change of voltage** if “**piezoelectric crystal**” is used as the transducer. (Detail descriptions available in Chapter 7)



Overview of Finite Element Stress Analysis (p.173)

Finite element method (FEM) is a powerful tool in stress analysis of MEMS and microsystems of **complex geometry**, **loading** and **boundary conditions**.

Commercial FEM codes include: **ANSYS**, **ABAQUS**, **IntelliSuites**, **MEMCad**, etc.

The essence of FEM is to **discretize** (divide) a structure made of continuum into a finite number of “**elements**” interconnected at “**nodes**.” Elements are of specific geometry.

One may envisage that **smaller and more elements** used in the discretized model produces better results because the model is closer to the original continuum.

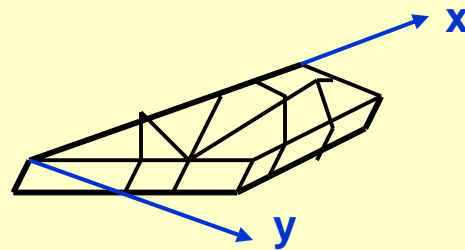
Continuum mechanics theories and principles are applied on the individual elements, and the results from individual elements are “assembled” to give results of the overall Structure.

I/O in FEM for Stress Analysis

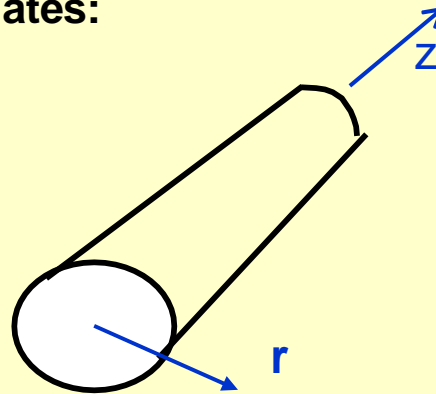
• Input information to FE analysis:

(1) General information:

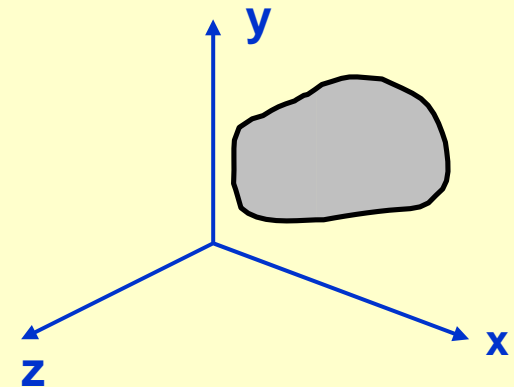
- Profile of the structure geometry.
- Establish the coordinates:



x-y for plane



r-z for axi-symmetrical



x-y-z for 3-dimensional geometry

(2) Develop FE mesh (i.e. discretizing the structure):

Use automatic mesh generation by commercial codes.

User usually specifies desirable density of nodes and elements in specific regions.

(Place denser and smaller elements in the parts of the structure with abrupt change of geometry where high stress/strain concentrations exist)

(3) Material property input:

In stress analysis: Young's modulus, E ; Poisson ratio, ν ; Shear modulus of elasticity, G ; Yield strength, σ_y ; Ultimate strength, σ_u .

In heat conduction analysis: Mass density, ρ ; Thermal conductivity, k ; Specific heat, c ; Coefficient of linear thermal expansion coefficient, α .

(4) Boundary and loading conditions:

In stress analysis: Nodes with constrained displacements (e.g. in x-, y- or z-direction); Concentrated forces at specified nodes, or pressure at specified element edge surfaces.

In heat conduction analysis: Given temperature at specified nodes, or heat flux at specified element edge surfaces, or convective or radiative conditions at specified element surfaces.

• Output from FE analysis

(1) Nodal and element information

Displacements at nodes.

Stresses and strains in each element:

- Normal stress components in x, y and z directions;
- Shear stress components on the xy, xz and yz planes;
- Normal and shear strain components
- Max. and min. principal stress components.
- The von Mises stress defined as:

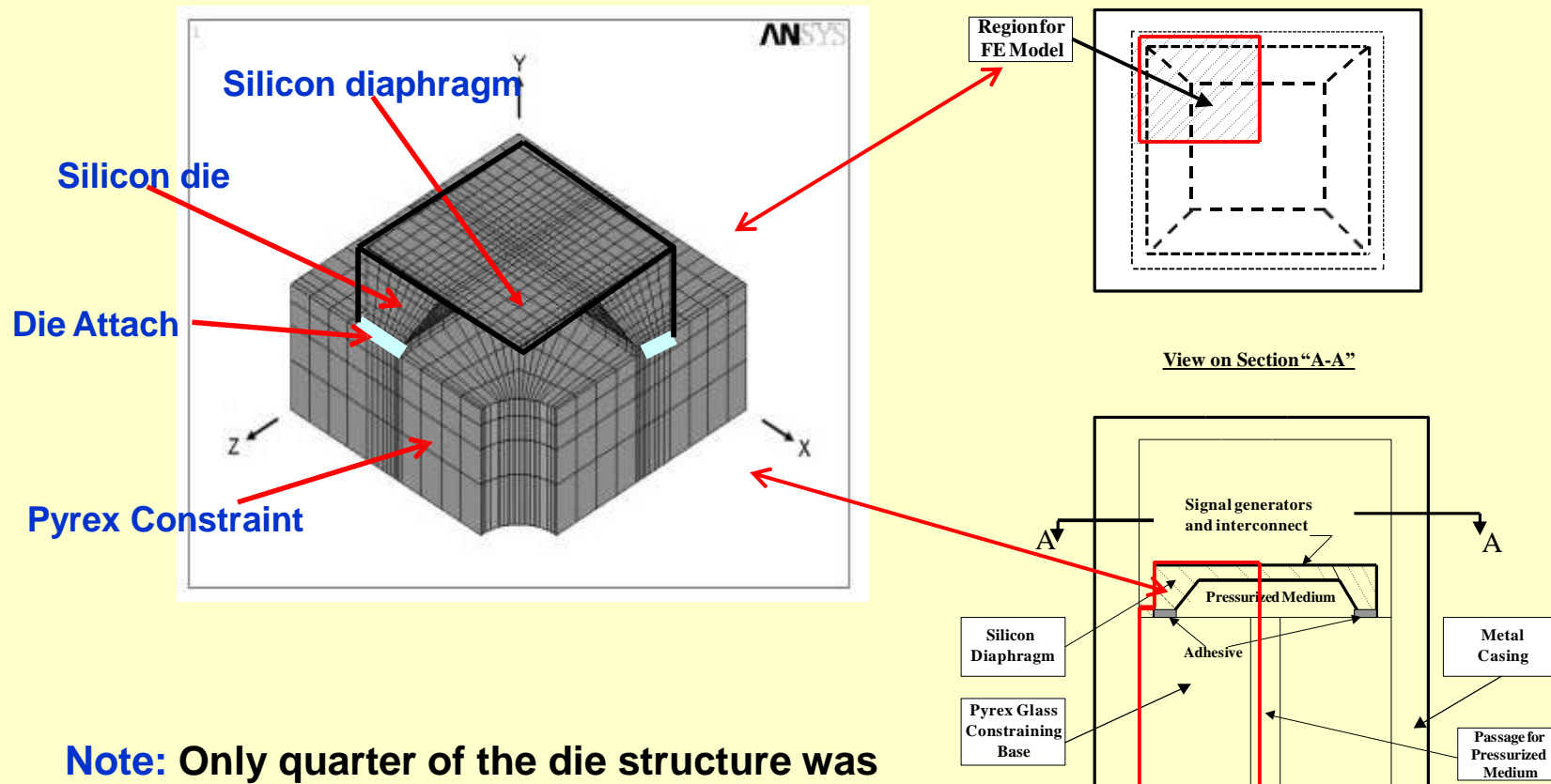
$$\bar{\sigma} = \frac{1}{\sqrt{2}} \sqrt{(\sigma_{xx} - \sigma_{yy})^2 + (\sigma_{xx} - \sigma_{zz})^2 + (\sigma_{yy} - \sigma_{zz})^2 + 6(\sigma_{xy}^2 + \sigma_{yz}^2 + \sigma_{xz}^2)} \quad (4.71)$$

The **von Mises stress** is used to be the “representative” stress in a **multi-axial stress situation**.

It is used to compare with the yield strength, σ_y for plastic yielding, and to σ_u for the prediction of the rupture of the structure, often with an input safety factor.

Application of FEM in stress analysis of silicon die in a pressure sensor:

by V. Schultz, MS thesis at the MAE Dept., SJSU, June 1999 for LucasNova Sensors
In Fremont, CA. (Supervisor: T.R. Hsu)



Note: Only quarter of the die structure was in the FE model due to symmetry in geometry, loading and boundary conditions.

modification. One such system, *profilometry*, was introduced earlier for measuring surface features after etching.

Many of the following methodologies are based on the sensor principles and clinical laboratory methods already introduced. Some may be used for *either* detection or characterization; and a few are suitable for integrating within a microfluidic chip, making them especially attractive for implanted medical micro-devices. Packaging, powering, and communicating with these specialized systems, and making them biocompatible is discussed in Chapter 14.

While a few specific applications are discussed here for illustration purposes, the recommended reading provides a broader understanding of the role of these techniques in bioMEMS.

10.2 Detection Schemes

10.2.1 Electrochemical (EC) detection

Electrochemical analysis in liquid solutions is concerned with the measurement of electrical quantities, such as potential, current, and charge in order to gain information about the composition of the solution and the reaction kinetics of its components. Various methods for EC detection were described in Chapter 6. Typically less expensive than the fluorescent techniques described below, EC detection in LOC devices has considerable value. The emerging technologies incorporate microfabrication of electrodes within the device as opposed to external electrodes.

Capillary electrophoresis devices were among the first to incorporate micro-fabrication of integrated electrodes. To illustrate the steps for accomplishing the work of Baldwin et al. (2002) is considered for developing a LOC device with integrated EC detection. Much of their work is built upon earlier efforts [Pai et al., 2001].

Both CE channels and all CE/EC electrodes were incorporated directly onto glass substrates via traditional microfabrication techniques, including photolithographic patterning, wet chemical etching, dc sputtering, and thermal wafer bonding. Critical electrode characteristics, including size, shape, and positions were fabricated into the chip, eliminating the need for external electrodes. Figure 10.1 shows the CE/EC device layout and the side view of the EC detection cells and electrodes. The four CE reservoirs (sample, waste, buffer, and detection) were formed by drilling through the upper glass substrate. The corresponding Pt CE electrodes were patterned onto the bottom plate. Channels were 20- μm deep, 50- μm wide, and 1-cm long.

To achieve the 250 V/cm electric fields required for the short-length CE tubes, Baldwin used a battery-operated power supply delivering 250 V and 2000 V dc for the injection and separation channels, respectively. EC detection was carried out amperometrically with a three-electrode potentiostat constructed from operational amplifiers and various passive components powered by a single 9-V battery.

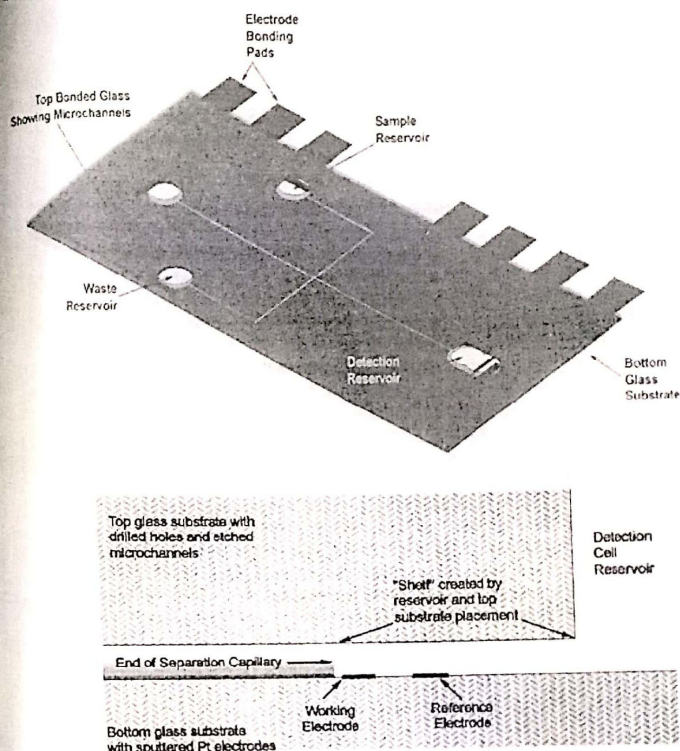


Figure 10.1 Capillary electrophoresis with electrochemical detection chip. (a) The CE/EC device layout, and (b) the side view of the EC-detection cells and electrodes. [Reprinted with permission from Baldwin et al. (2002), copyright American Chemical Society.]

The CE electrodes consisted of 0.3- μm thick, 2.2-mm wide, and 6.9-mm long Pt deposits placed in each of the CE reservoirs, located as far as possible from the CE channels to minimize the possibility that any bubbles that might form and disturb the flow of fluid. EC electrodes consisted of 0.3- μm thick Pt deposits placed in the detection reservoir only. The working and reference electrodes were 40 μm wide semicircular Pt "fingers" located in various positions.

Catechols were selected for separation and detection, and performance was similar to hybrid devices with external CE or EC electrodes.

Another application area of EC is the detection of organisms to diagnose disease, prevent food poisoning, and alert to bioterrorism threats. Several techniques for bacterial detection, including EC, SAWs, optical and molecular beacons, and aptamers are reviewed by Deisingh and Thompson (2004).

10.2.2 Chemiluminescence and bioluminescence

Chemiluminescence (CL) is the generation of light (visible, ultraviolet, and infrared) caused by the release of energy from a chemical reaction, and was discussed in Chapter 8. Unlike fluorescence, where an excitation source is needed and non-specific radiation can be produced, CL occurs only when the reactants are present, and noise is inherently low.

Detection of hybridizations using enzyme-catalyzed CL reactions and a microchannel glass array has been performed by Cheek et al. (2001). A "flow-thru" chip consisting of a 3D-ordered set of microchannels and a microarray platform was fabricated as shown in Fig. 10.2. Analyte-specific reagents, or probes, are deposited on the chip in an array of spots. Each spot incorporates several individual channels, and imaging was accomplished with a CCD camera.

Rapid bacterial detection is also possible using CL techniques. Ozen et al. (2004) harness the specificity of bacterial phage for their host with a modified quorum-sensing amplification signal, to produce quantifiable bioluminescent detection on a silicon *microluminometer*. Envisioned are μ TAS microbial contamination monitors as part of an environmental control system with on-chip signal processing and network interfacing.

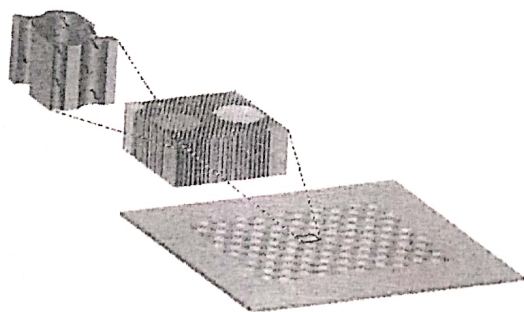


Figure 10.2 Conceptual schematic of a microchannel glass array connected to a planar surface for detection. [Reprinted with permission from Cheek et al. (2001), copyright American Chemical Society.]

10.2.3 Fluorescence

When illuminated at different wavelengths, some molecules emit light of a different color. For example, fluorescein dye emits green light when illuminated with blue light. The molecules absorb the higher-energy blue light then lose some of the energy in the form of lower-energy photons—here, green light. Dyes, excitation energy, and attachment to the target molecule can all be modified for specific analysis.

A fluorescent microscope is shown schematically in Fig. 10.3. Excitation light is reflected off a dichroic mirror, through the objective lens onto the sample. Dichromatic mirrors reflect light shorter than a certain wavelength, and pass light longer than the wavelength. Fluorescence from the sample is collected by the object lens and, being of longer wavelength (lower energy), passes back through the dichroic mirror to a detector (or human eye).

Epifluorescence involves illuminating the specimen from above while in trans- fluorescence the excitation light comes from below the sample [Weeks, 2004].

LOC laser devices (including use of optical fibers) have been developed by a number of investigators and offer the potential for on-chip excitation, see for example Helbo et al. (2004), Jensen-McMullin et al. (2002), Lamontagne (2003), Nilsson et al. (2004), Thrush et al. (2002), and Yang et al. (2000).

Integrated optical detection used for fluorescence measurement has also been accomplished by Boppart et al. (2002), Cui et al. (2002), Thrush et al. (2002), and Yang et al. (2000).

Design, fabrication, and characterization of a disposable integrated microfluidic device with self-aligned planar microlenses, light-emitting diodes (LEDs) as excitation sources, and photodiodes as detectors is described by Seo and Lee (2004). The optical detection is based on the orthogonal arrangement of excitation light via a 2D planar microlens integrated onto the microfluidic channel that collects the fluorescent emission. This provides an effective detection mechanism

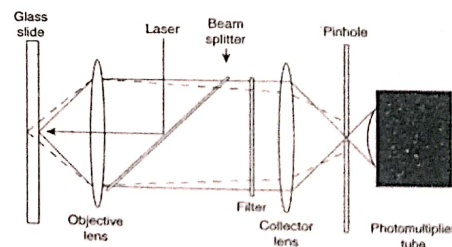


Figure 10.3 Fluorescent microscopy is used in the confocal scanning laser microscope. The addition of a pinhole removes light that is out of the plane with the desired sample. Additional mirrors are used to scan the entire sample, and signals must be digitally reconstructed. [Reprinted with permission from Baldi and Hatfield (2002), copyright Cambridge University Press.]

with an increased signal-to-noise ratio, minimal optical aberration, amplified fluorescence, and self-alignment of the micro-optical system. LED-based fluorescence is also reviewed by Dasgupta et al. (2003). Camou et al. (2002) describes a novel application using organic light-emitting diodes (OLED) as an excitation source for the optical detection based on fluorescence spectroscopy.

Miniaturized electrophoresis has been successfully coupled with native fluorescence detection for direct analysis of proteins in 1D and 2D separations. Slusny et al. (2004) performed detection based on direct observation of the UV-induced fluorescence of proteins using a CCD camera and an Hg (Xe) lamp for sample excitation.

Tung et al. (2004) describe the design and performance of a microfluidic observation channel capable of performing flow cytometry measurements through the use of solid-state lasers and PIN-based photodetectors. The observation cell, made of PDMS, was fabricated with integrated *microgrooves* that permit the physical registration of optical fibers that serve as optical waveguides for laser excitation and fluorescence detection. The technique is applicable to the detection of scatter and fluorescent signals emanating from inorganic particles and biological cells, and μ TAS.

High-throughput analyses may be achieved with μ TAS. Chartier et al. (2003) describe an automated genotyping system based on continuous flow analysis, which integrates all the steps of the genotyping process (PCR, purification, and sequencing). The genotyping device consists of a disposable hybrid silicon-plastic microfluidic chip, equipped with a permanent external, heating/cooling system; syringe-pump-based injection systems; and on-line fluorescence detection. High throughput is obtained by performing the reaction in a continuous flow and in parallel (48 channels) [Chartier et al., 2003]. Thrush et al. (2003) also describe high-throughput analysis using VCSELs, optical emission filters, and PIN photodetectors to realize monolithically integrated, near-infrared, fluorescence detection systems.

10.2.4 Molecular beacons (MBs)

Molecular beacons (MBs) are single-stranded oligonucleotide hybridization probes that form a stem-and-loop structure. The loop contains a probe sequence that is complementary to a target sequence, and the stem is formed by the annealing of complementary arm sequences that are located on either side of the probe sequence. Figure 10.4 shows the molecular beacon and target hybridization. A fluorophore is covalently linked to the end of one arm, and a quencher is

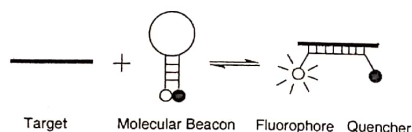


Figure 10.4 Molecular beacon and target hybridization.

covalently linked to the end of the other arm. When MBs hybridize to the appropriate target nucleic acid stands, the probe transitions from dark to fluorescent as conformational changes move the fluorophore away from the nonfluorescence quencher. This is known as fluorescence resonance energy transfer. When the probe encounters a target molecule, it forms a probe-target hybrid that is longer and more stable than the stem hybrid.

Multiple assays may be performed simultaneously by using up to seven different colored fluorophores specific for different targets. MBs are very specific and can distinguish a single nucleotide substitution; thus, they are ideal probes for use in diagnostic assays designed for genetic screening, detection of single-nucleotide polymorphisms, and pharmacogenetic applications [Kramer, 2004]. They are limited, however, in specificity of protein recognition.

10.2.5 Aptamers

Aptamers are artificial nucleic acid ligands that can be generated against amino acids, drugs, proteins, and other molecules. They are isolated from complex libraries of synthetic nucleic acids by an iterative process of adsorption, recovery, and amplification [Luzi et al., 2003]. Aptamers are single-stranded DNA molecules that fold into 3D shapes through which they can discriminate proteins or other molecules in highly specific affinity interactions. Incorporation of photoreactive 5-bromodeoxyuridine (BrdU) creates a *photoaptamer* and covalently cross-links the photoaptamer to a bound protein by irradiating it with 308-nm light [Bock et al., 2004].

When used as a capture-molecule, detection is achieved with a fluorescently labeled antibody to the cross-linked complex.

Aptamers may be synthesized through a process known as *photochemical systematic evolution of ligands by exponential enrichment* (PhotoSELEX) [Golden et al., 2000]. An affinity SELEX process is described by Petach and Gold (2002), and is shown in Fig. 10.5. Protein targeted molecules are bound to

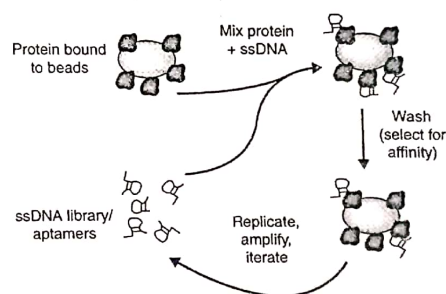


Figure 10.5 Affinity SELEX process. [Reprinted with permission from Petach and Gold (2002), copyright Elsevier.]

magnetic beads and reacted with single-stranded DNA (ssDNA) libraries to select ssDNA that binds to specific protein targets without being removed by washing the beads. The high-affinity ssDNA that remains bound is subsequently amplified by PCR and cycled again for enrichment.

10.3 Measurement Systems

10.3.1 Confocal laser microscopy

Confocal scanning laser microscopy has significant utility for DNA microarray chips and other LOC devices. Normally, in simple fluorescence microscopy the entire sample is illuminated by the excitation light, causing the entire sample to fluoresce, thereby creating a blurred image. Refer back to Fig. 10.3, where the addition of a pinhole filters out light that is out-of-plane with the desired light. The object lens forms an image at the pinhole surface, and the sample and pinhole planes are known as conjugate planes. The pinhole is *conjugate* to the focal point of the lens thus the term *confocal* laser microscopy. As in fluorescence microscopy, light from the laser (higher wavelength) is reflected by the dichroic mirror through the objective lens onto the sample. The fluorescence (lower wavelength) is gathered by the objective lens, passes through the dichroic mirror and is focused onto the pinhole surface. A photomultiplier tube measures the fluorescent energy. Moving mirrors allow the entire sample to be scanned [Weeks, 2004].

Figure 10.6 shows the Berkeley Rotary Confocal Fluorescence Scanner configured for μ CAE detection, where laser excitation at 488 nm is reflected by a dichroic beamsplitter through a hollow shaft stepper motor and deflected 1.0-cm off-axis by a rhomb prism mounted on the motor shaft. Laser excitation is focused and fluorescence is collected by the microscope objective, and reflected back through the beamsplitter back to the detector. Fluorescence is spectrally filtered (dichroic beamsplitter and bandpass filter), spatially filtered (pinhole) and four-color processed. Each bandpass filter has 20-nm-wide bands centered at 650, 580, 550 and 520 nm, respectively [Blazej et al., 2003].

A two-mirror microscanner suitable for building a miniaturized confocal laser scanning microscope has been described by Hoffman et al. (1999). The electrostatically driven torsional micromirrors are suitable for fast 2D scanning with high angular precision over large scan angles. The planned initial use is for improved imaging at the tip of an endoscope.

10.3.2 Interferometry

Interferometers are measuring instruments that take advantage of the physical phenomena of *interference patterns*. Interference occurs with the superposition of two or more electromagnetic waves. For coherent visible light (wavelengths of 450 to 700 nm) with similar frequency and phase, and traveling in the same direction, this may be observed as bands or *fringes* of light and dark, which

DETECTION AND MEASUREMENT METHODS

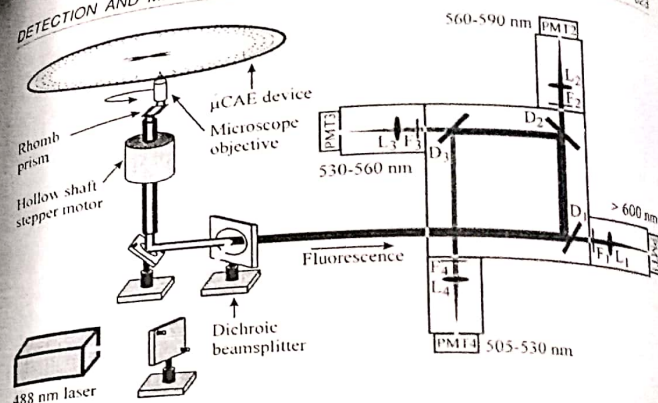


Figure 10.6 The Berkeley rotary confocal fluorescence scanner used to interrogate radial micro capillary array electrophoresis devices. (a) Laser excitation at 488 nm is reflected by a dichroic beamsplitter through a hollow shaft stepper motor and deflected 1.0-cm off-axis by a rhomb prism mounted on the motor shaft. Laser excitation is focused and fluorescence is collected by the microscope objective, and reflected back through the beamsplitter back to the detector. (b) Fluorescence is spectrally filtered (dichroic beamsplitter and bandpass filter), spatially filtered (pinhole) and four-color processed [Reprinted with permission from Oosterbroek and van den Berg (2003); copyright Elsevier]

are based on addition or subtraction of wave components at a given point. These are referred to as *maxima* and *minima*.

Historically, interference helped establish the wave nature of light. Observations of colored fringe patterns on thin films were among the first observations of interference. In 1801, Thomas Young derived a method called the *double-slit experiment* whereby interference patterns could be obtained without having a coherent light source (lasers had not yet been invented!). One wavefront as derived by light passing through a single slit was made to pass through two parallel slits less than a millimeter apart, creating two coherent wavefronts whose interference pattern could be observed on a screen one to two meters away. *Diffraction* occurs whenever a wavefront is obstructed, such as passing through a single slit, with resulting alteration of amplitude and phase. Fringes or diffraction patterns are formed as some electromagnetic radiation bends around the obstacle into the shadow and mutually interfere.

The Michelson interferometer produces interference fringes by splitting a beam of monochromatic light so that one beam strikes a fixed mirror and the other a movable mirror. The beams are reflected back to a common target producing interference patterns.

Young was also able to explain the phenomenon known as *thin-film interference*, something we observe when looking at the different colors on soap bubbles, oil spots, or metallic surfaces. A thin film will divide an incoming wavefront into three components: (1) light reflected from the top surface; (2) light reflected from the bottom surface; and (3) light transmitted through the material. The two reflected waves create an interference pattern on an observer's retina.

In modern optics, similar waves are usually derived by splitting a single *coherent light* source and bending the split beam with front-silvered mirrors and prisms. Coherent light is typically obtained by a gas laser or solid-state *laser-emitting diode* (not to be confused with a *light-emitting diode* (LED), which emits incoherent light).

Very sensitive detectors for measuring wavelengths, small distances, vibrations, and surface flatnesses can be produced using interferometry. Interferometers may be used to measure dynamic displacement of micropump actuator surfaces and other dynamic bioMEMS processes [Husband et al., 2004; Tomac et al., 2002; Rembe et al., 2001]; identification of chemical weapons of mass destruction and other hazardous materials based on Fourier transform infrared (FT-IR) spectroscopy [Norman et al., 2004]; and for precise positioning for fabrication based on ion-projection lithography [Loeschne et al., 1994].

Interference-based integrated optical sensors such as the *Mach-Zehnder interferometer* and the *Young interferometer* are among the most sensitive devices, which are able to detect refractive index changes as small as 10^{-8} . This corresponds to a protein concentration of 5.3×10^{-8} g/ml. The high sensitivity, combined with fast and accurate measurement, makes these devices very attractive for μ TAS. For example, an integrated optical four-channel Young interferometer microfluidic chip has been shown to be useful for immunosensing applications [Ymeti et al., 2004].

10.3.3 Ellipsometry

An ellipsometer is a special arrangement of polarizers, phase retarders, light sources, and detectors for the generation and analysis of polarized light. It may be used to measure optical properties and surface properties of materials and thin films.

In *plane-polarized* electromagnetic radiation, all the electronic oscillations are parallel to each other and at right angles to the magnetic oscillation. Light can be plane-polarized by reflection or by passing through certain substances such as a Polaroid filter. *Elliptical polarization* consists of two plane-polarized radiations traveling together, out of phase by 90 deg, and of unequal magnitude [Daintith and Clark, 1999]. In an ellipsometer, laser light is used as the source, and retarders shift the phase of one component of the incident light. If a light beam illuminates a thin film/substrate surface under oblique incidence, reflection from the surface changes the ellipse of polarization.

In imaging ellipsometry, the incident light is still provided by a collimated laser beam, but an imaging system is added to gather the reflected light. This system consists of an objective lens and a spatially resolving detector such as a sensitive CCD camera. The detected signal is spatially resolved showing the sample

details. A motorized focusing mechanism collects a series of images with different foci within the field of view. Superimposing the images with digital image processing, results in a sharp edge-to-edge image.

10.3.4 Surface-plasmon-resonance spectroscopy

Surface-plasmon-resonance (SPR) measurements are made using optical systems that control the angle and wavelength of incident light and the degree of polarization. This technique is commonly used to study ultrathin films, and may be used to characterize immobilized molecules in bioMEMS devices.

A combination of substrate, noble metal, and sample in contact with the metal allows for the generation and support of surface-plasmon polaritons (SPPs). These are formed along the metal-dielectric interface, and are highly damped charge density waves that oscillate at optical frequencies, and may be excited if the materials and optical properties of an experimental system are chosen correctly.

SPPs are not measured directly, but their presence is inferred by monitoring the light intensity reflected from the substrate/metal interface. The reflected light contains a deep minimum in intensity, which occurs at what is termed as the resonance for the surface polariton, or plasmon. The monitoring of the surface plasmon reflectivity curve, and in particular, the position of the resonance, yields what is generally known as surface-plasmon-resonance spectroscopy (SPRS). The position of the reflectivity minimum is very sensitive to the interface properties between the substrate face and the liquid. Changes in metal film thickness, surface adsorbed species, and liquid dielectric properties are all seen as changes in the SPR wavelength. SPR has been shown to be sensitive to very low levels of material adsorbed onto a surface [McWhorter et al., 2003].

10.3.5 Raman microscopy (RS) and surface-enhanced resonance Raman scattering (SERRS)

Raman microscopes use the *Raman effect* to identify and characterize the chemistry and structure of materials in a no-contact, nondestructive manner. The Raman effect occurs when laser light is shined on a material and light is scattered, a tiny fraction of which is shifted in frequency as atoms in the material vibrate. Analysis of the frequency shifts (spectrum) of the light reveals the characteristic vibration frequencies of the atoms and hence the chemical composition and structure of the material. Particles of $1 \mu\text{m}$ can be uniquely identified.

The frequency shift is determined as follows [Poole and Owens, 2003]:

$$\Delta\omega = \omega_{\text{phonon}} = |\omega_{\text{inc}} - \omega_{\text{scat}}|,$$

where

ω_{phonon} is the optical phonon mode vibration,
 ω_{inc} is the incident light frequency, and
 ω_{scat} is the scattered light frequency.

In Raman microscopy the sample is typically illuminated with a laser and the light scattered by the material is analyzed by a conventional optical microscope coupled to a *Raman spectrometer*. The Raman frequency shift is analyzed at different points in the sample, and is able to resolve parts with different chemical composition in a sample. It may be used for analysis of thin films, coatings, microelectronic integrated circuits, mineral inclusions, biological tissues, and identification of narcotics and plastic explosives.

Surface-enhanced resonance Raman scattering (SERRS) yields information about the molecular structure of an analyte in the form of a *vibrational spectrum*. The frequency of the excitation source is tuned to be in resonance with an analyte. SERRS is an advancement of Raman spectroscopy and surface-enhanced spectroscopy by adsorbing target molecules onto silver colloid nanoparticles and applying excitation energy.

Keir et al. (2002) describe a technique for producing the required SERRS silver colloid substrate *in situ* in microfluidic channels. An aggregated silver colloid is prepared by borohydride reduction of silver nitrate. Ports for infusing an azo dye derivative of trinitrotoluene (TNT) solution as analyte, silver nitrate and sodium borohydride were fabricated in the LOC device. The preparation results in a thin line of colloid (about 30- μm wide) that remains stable over extended periods of time and is suitable for detection with a Raman microscope, which collects signals from a small volume. Detection of as little as 10 fmoles of the azo dye was possible. The investigators envision a portable-explosive detection device using such technology.

The development of ultra-sensitive spectroscopic techniques now makes possible the detection and the identification of single inorganic and organic molecules. By approaching the single molecule level, phenomena usually hidden due to ensemble averaging can be directly observed and, in addition, the real dynamic behavior of the biomolecule can be followed [Bizzarri et al., 2002].

Grow et al. (2003) describe a surface-enhanced Raman scattering (SERS) μTAS for label-free detection of pathogens and their toxins. The μSERS process consists of an array of capture biomolecules immobilized on a SERS-active metal surface combined with a Raman microscope to collect the SERS fingerprints. Figure 10.7 shows the flow diagram of the μSERS process. Their initial studies have shown that the gram-positive *Listeria* and gram-negative *Legionella* bacteria, *Bacillus* spores, and *Cryptosporidium* oocysts can often be identified at the subspecies/strain level on the basis of SERS fingerprints collected from single organisms. The physiological state of bacterial cells and toxins could also be uniquely detected by their SERS fingerprint.

10.3.6 Transmission electron microscopy (TEM) and scanning electron microscopy (SEM)

The transmission electron microscope (TEM) was invented more than seventy years ago by Knoll and Ruska (1932), who were driven by the desire to overcome the limitations of light microscopy. Light microscopes are limited by the physics of

DETECTION AND MEASUREMENT METHODS

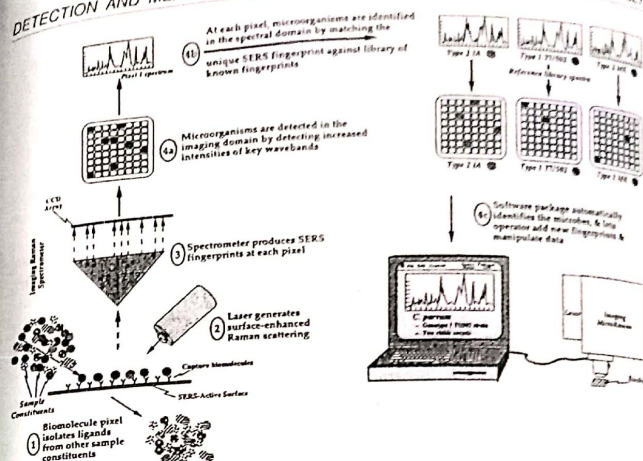


Figure 10.7 Flow diagram of the μSERS process. [Reprinted with permission from Grow et al. (2003), copyright Elsevier.]

light, allowing about 1000 \times magnification with a resolution of about 0.25 μm . It is now possible to achieve 1- \AA TEM image resolution with concomitant atom-position information.

Electron microscopes use a focused beam of electrons for imaging rather than light. Scanning electron microscopes (SEM) use a "scanning" beam of electrons across the sample, making it possible to study the *topology*, *morphology*, *composition*, and *crystallographic* qualities of materials. Topology includes surface features and texture from which such properties as hardness and reflectivity may be inferred. Morphology is the shape and size of the particles making up an object from which such properties as ductility, strength, and reactivity may be inferred. Composition includes the elements and compounds that compose an object and their relative abundance from which such properties as melting point, reactivity, and hardness may be inferred. TEM is the primary tool for the observation of crystal defects including dislocations, grain boundaries, interphase interfaces, and other planar defects that control mechanical, chemical, physical, magnetic, and electrical properties of materials.

TEM may be coupled with x-ray detectors and electron spectrometers (STEM) allowing quantitative analysis of almost all of the elements with a spatial resolution of nanometers and sensitivity approaching single-atom levels. Compositional maps may be achieved with energy-filtered electron imaging and x-ray mapping. The digital combining of these image planes, along with the traditional image and diffraction planes, may be used to generate various *maps*.

including elemental chemistry, local atomic bonding, dielectric constant, specimen thickness, and band gap. TEM is perhaps the most complete *analytical tool* available to the materials researcher [Newbury and Williams, 2000].

Commercial SEMs appeared about 25 years after TEMs. They have a coarser resolution, in the 20–50 nm range, which is limited by a combination of the incident-probe diameter and the scattering of the beam of electrons within the target. They are lower cost and simpler to use than the TEMs. The 3D images of SEM do not require an extensive theoretical and calculation base to perform meaningful image interpretation. Contrast information derives primarily from surface topography or local compositional differences. Environmentally controlled SEMs allow examination of specimens without application of conducting coatings usually necessary for imaging in high vacuum SEMs and TEMs. Dynamic experiments are possible with an SEM because of the large specimen stage and the longer working distance between the objective lens and the focal plane, which ranges from 1 to 6 cm [Newbury and Williams, 2000].

10.3.7 Atomic force microscopy (AFM)

Atomic force microscopy (AFM) is a form of *scanned-proximity probe microscope* in which measuring a local property such as height, optical absorption, or magnetism is performed by placing a probe near the sample. The probe-sample separations are on the order of the system resolution, and imaging occurs by raster scanning the surface of interest.

AFM measures topography with a force probe, and operates by measuring the attractive or repulsive forces between a probe tip and the sample. Unlike a stylus profilometer, the AFM is measuring hard-sphere repulsive forces between the tip and sample, and incorporates a positioning feedback loop. In *contact mode* a cantilever tip lightly touches the sample while deflection of the cantilever is measured and related to height. Measuring cantilever deflection with the angular deflection of a laser beam allows picometer resolution. This technique may be used in the presence of water. In *noncontact mode* the tip does not touch the sample, but instead measures the attractive forces.

Cantilevers and probe tips are typically manufactured by micromachining. Sample positioning in 3D below the tip is precisely done with piezoelectric positioners. While x-y positioning provides for raster scanning, feedback compensation along the z-axis allows nearly constant cantilever beam deflection and hence faster imaging. Topography is determined by the sum of the z-axis compensation and the error signal (the latter is presumably negligible).

An alternative methodology is to measure cantilever torsional deflection as friction between the tip and sample cause the cantilever to twist. This lateral force data may be combined with the topographical image to yield additional information.

Sample elasticity can be measured by holding the x-y axis stationary while the tip presses into the sample, and cantilever deflection is measured. This technique is useful for biologically modified surfaces [Baselt, 1993].

Recent advances in AFM allow one to perform complex analyses of material surfaces and near-surface regions with a nanometer scale resolution. This includes the imaging of surface topography and the measurements of stiffness, elasticity, hardness, and nanotribological characteristics.

10.4 Review Questions

1. Show diagrammatically how capillary electrophoresis is accomplished in a bioMEMS device and where electrochemical detection would be integrated.
2. Define each of the following terms: (1) chemiluminescence, (2) bioluminescence, and (3) electrochemiluminescence.
3. Explain how fluorescence works and how this may be used as a method of detection in a bioMEMS device.
4. Show diagrammatically how molecule beacons function and explain how they may be useful in performing multiple assays simultaneously.
5. What are aptamers, how are they created, and by what means are they detected?
6. Show diagrammatically how a confocal laser microscope functions and explain the function of each component. What is meant by confocal?
7. What is Young's double-slit interferometer? List some uses for interferometry in bioMEMS devices.
8. Describe how an ellipsometer functions.
9. What is surface-plasmon-resonance spectroscopy?
10. Describe the Raman effect and how it is used in surface-enhanced resonance Raman scattering (SERRS) measurements.
11. How are electron microscopes useful? Describe how they operate, and distinguish between transmission electron microscopy and scanning electron microscopy, both in operation and application.
12. What does an atomic force microscope measure, and how does it operate?

References

- Baldi, P. and G.W. Hatfield, *DNA Microarrays and Gene Expression*. Cambridge University Press, Cambridge, UK (2002).
- Baldwin, R.P. et al., "Fully integrated on-chip electrochemical detection for capillary electrophoresis in a microfabricated device." *Analytical Chemistry* 74(15), pp. 3690–3697 (2002).
- Baselt, D., "The tip-sample interaction in atomic force microscopy and its implication for biological applications." Ph.D. diss., California Institute of Technology (1993).